The evolution of electrochemical, microstructural, and mechanical properties of aluminium alloy 2024-T4 (D16AT) during fatigue cycling

S R Salimon[1], **A I Salimon**[1], and **A M Korsunsky**[2*]
[1]Moscow Institute of Steels and Alloys, Moscow, Russia
[2]Department of Engineering Science, University of Oxford, Oxford, UK

The manuscript was received on 15 July 2008 and was accepted after revision for publication on 21 September 2009.

DOI: 10.1243/09544100JAERO423

Abstract: Coupons of fuselage skin made from the aluminium alloy D16AT (the Russian equivalent of 2024-Ò4) were obtained from several Russian TU-154 passenger aircraft after different numbers of flight cycles and different lengths of operation. The coupons were subjected to electrochemical, microstructural, and mechanical testing with the aim of identifying any trends indicating fatigue damage accumulation and residual fatigue lifetime reduction during service. Alongside this investigation, laboratory fatigue test specimens were machined from the same alloy and subjected to cyclic fatigue loading to simulate the service conditions for the coupons. Electrochemical testing was used in order to determine the evolution of the corrosion potential of the near-surface layers. X-ray diffraction analysis was also carried out to characterize residual stress and texture evolution, while microstructural investigations were made using transmission electron microscopy (TEM), scanning electron microscopy (SEM), and secondary ion mass spectroscopy. The suitability of using electrochemical, microscopic, and diffraction characterization methods for the detection of surface structural state modification and its connection with the mechanical performance of this alloy are discussed.

Keywords: fatigue, corrosion, electrochemistry, ageing aircraft

1 INTRODUCTION

In recent years, the problem of aircraft lifetime extension has become the subject of much attention, owing to the increasing pressures on airline companies to provide ever greater amounts of passenger movement at price levels that continue to be pushed down by competition. The situation is particularly critical for developing countries and countries of the Newly Independent States. In many instances, economic difficulties in these countries prevent them from buying newly built aircraft. This results in the ongoing use of the existing planes after periods approaching the original estimates of their safe operating lifetime. In Russia, about 80 per cent of civil aircraft are currently being flown at the 80–90 per cent lifetime level. Some smaller companies continue to exploit aircraft beyond their normal operating lifetime. This extended use poses serious problems of ensuring flight reliability for civil air companies.

In this situation, the methods of non-destructive damage diagnostics for aircraft structural materials assume great importance. In Russia, recent years have shown a sharp increase in the interest in the problems of assessing aeroplane ageing, and the development of methods for reliable and certifiable lifetime extension. While the majority of passenger aircraft have seen 25–30 years of service, the likelihood of their replacement in the near future remains low. Airlines attempt to identify suitable guidelines for the extension of safe operating time, based on scientifically justified and verifiable grounds.

The problem of identifying suitable criteria for estimating residual lifetime of aircraft can be separated into two specific sub-tasks, with characteristic methodologies.

1. Diagnostic procedures aimed at detecting major intolerable damages (internal cracks, ruptures, or

*Corresponding author: Department of Engineering Science, University of Oxford, Parks Road, Oxford OX1 3PJ, UK.
email: alexander.korsunsky@eng.ox.ac.uk

corrosion pits) during routine inspection between flights.
2. Complex integrated procedures for continuous non-destructive monitoring of all elements and assemblies in an aeroplane, where the probability of intolerable damages emerging directly during flight is high.

In the present study, the focus is on sub-task 2 in particular. In order to develop and adopt this methodology, it has to be assumed that some reliable accelerated tests may be devised that are capable of determining structural weaknesses, e.g. locations where dangerous fatigue cracks have appeared or may initiate in the time between inspections. If such tests can be formulated and established, they would also provide powerful tools for the estimation of safe residual lifetime.

The development of residual fatigue lifetime monitoring tests must be based on some suitable models of cyclic evolutionary response to fatigue loading in structural materials and components, at different structural levels (phase state, dislocation structure, grain ensemble, chemical inhomogeneity, electron subsystem, etc.). However, it is notoriously difficult to construct a simple, but realistic, picture of fatigue response evolution, owing to the synergetic nature of fatigue damage accumulation. As far as normal operation in civil aviation over periods of several decades is concerned, the conditions of service are particularly difficult to describe and simulate with adequate reliability. Indeed, in many cases complementary influences must be considered of high- and low-cycle fatigue (HCF–LCF interaction), electrochemical corrosion and wear.

Nevertheless, arguments built on physically justified assumptions may be put forward, and attempts at their experimental verification be made. Dislocation activity in the very near-surface layers during high-cycle fatigue for which there is extensive evidence (e.g. reference [**1**]) induces modifications of the surface layer structural state. Continuous generation of high dislocation densities within microscopic volumes localized near the surface affects the character of alloy–environment interaction, which results in changes of the surface chemical state. Similarly, grain-level plasticity results in a complex evolution of intergranular stresses, characterized by the repeated stages of stress accumulation and relaxation, and eventual loss of continuity, crack initiation and failure. These processes can be detected with the aid of X-ray diffraction pattern analysis, which allows one to extract information about orientation and grain-group-specific microstresses and microstrains, and texture development.

The aluminium alloy 2024-T4 (D16AT in the Russian nomenclature) was chosen as a representative aircraft structural material for the present research. This alloy is widely used for various aeroplane components, such as fuselage skin and flanks. In order to identify a suitably sensitive technique for accelerated tests, a variety of experimental techniques were applied in this study. The purpose of the study was to detect structural changes induced by fatigue in this alloy. Mechanical property evolution was monitored for comparison.

In the present article, particular emphasis is placed on the use of electrochemistry for express diagnostics and monitoring. Electrochemical methods offer a number of important advantages:

(a) simplicity of operation;
(b) the possibility of using portable devices;
(c) relative cheapness;
(d) relative simplicity of interpretation.

Attempts have already been made previously to use electrochemical tests to analyse the property evolution in structural materials. The potential efficiency and reliability of these techniques have been reported in a number of studies [**2**]. In recent decades, passivation and pitting and the localized corrosion and corrosion inhibition of Al and Al alloys have been the subject of intense interest in the context of the aerospace industry, namely, the design, manufacture, and structural health monitoring in service. It has been suggested that anodic oxide films play an important role in controlling the corrosion resistance of the base metal. Aggressive anions such as chloride are believed to cause passive film breakdown, although the exact mechanism remains unclear [**3**]. A number of models have been proposed to explain passive film breakdown or pit initiation [**4**–**7**]. Three main models are:

(a) the adsorption mechanism;
(b) the penetration mechanism;
(c) the film breaking mechanism.

These models have been reviewed in depth in the literature [**8**, **9**].

Four stages of pitting corrosion can be distinguished [**9**]:

(a) processes occurring at the surface of the passive film, at the boundary of the passive film and the solution;
(b) processes occurring within the passive film, when no visible microscopic changes occur in the film;
(c) formation of the so-called metastable pits that initiate and grow for a short period of time below the critical pitting potential and then repassivate (this is an intermediate step in pitting);
(d) stable pit growth, above a certain potential termed the critical pitting potential. Metastable pits were first described qualitatively almost 50 years ago, but quantitative studies were not reported until the 1980s [**10**].

Szklarska-Smialowska [**11**] and other researchers reported oscillations of current anodic polarization curves and a constant potential below the pitting

potential for different metals and alloys in chloride solutions. The occurrence of these oscillations was explained by the consecutive formation and re-passivation of micro-pits that are very small in size and grow and re-passivate in less than a few seconds. Knowledge of the processes during the formation and re-passivation of the pits is helpful in understanding the processes that determine the stable growth of pits. The most important issues in the metastable pit studies are the processes leading to the formation of metastable pits and the electrochemical factors that influence the transition from metastable to stable pits.

Godard [**12**] investigated pit growth kinetics on aluminium and found that the pit depth was proportional to $t^{1/3}$, where t denotes the process time. Using this relationship good agreement with the pitting observed in service could be obtained. Hunkeler and Boehni [**13**] measured the time required for pits to perforate aluminium foils of different thickness in chloride solutions and found that the pit growth is ohmically controlled, since pit growth rate was related to the conductivity of the bulk electrolyte.

Intermetallics in Al alloys are either intentionally developed to obtain the desired mechanical properties or are present in the alloys as natural impurities. Although the addition of alloying elements increases the strength of aluminium, it dramatically decreases the corrosion resistance of the metal, e.g. to sea water. Some alloying elements, such as copper, have limited solubility in aluminium and are not uniformly distributed throughout the grains of the aluminium phase [**14**]. During precipitation hardening areas around the grain boundaries become depleted in copper and hence become more anodic (reactive) than the rest of the grain, promoting intragranular and intergranular corrosion. Depending upon the alloy, different second-phase particles are present [**15**]. For example, 1xxx alloys contain Al_6Fe and Al_3Fe, and 3xxx contain AlMg and AlMnMg particles. Intermetallics present in the alloy may decrease significantly the resistance to localized corrosion, notably particles with Cu and Fe in 2xxx and 1xxx alloys, respectively, while some other intermetallic particles do not seem to affect adversely the corrosion resistance. The effect of the intermetallic particles mainly depends upon the potential difference between the particle and the matrix in a solution. The phases that are electrochemically more noble than the matrix play the role of cathodes, so that the matrix undergoes anodic dissolution [**9**]. Buchheit [**16**] collected the corrosion potential values for intermetallic phases (mainly in NaCl solutions) common in Al alloys that can help predict the galvanic cell formation in Al alloys.

The behaviour of Al_2Cu at the open circuit potential and under anodic polarization in sulphate solutions was studied [**17**, **18**] and dissolution of this intermetallic was observed with the formation of Al^{3+} and Cu^{2+} that are produced by reduction on the electrode in the range of potentials corresponding to the stability of metallic copper. Electrochemical studies on synthetic Al_2Cu showed that these particles are cathodic with respect to aluminium [**19**].

Buchheit *et al.* [**20**] studied the behaviour of AA 2024-T3 in 0.1 M NaCl at pH 4.2. Four principal types of particles were found: 60 per cent AlCuMg (S-phase), 12 per cent Al (Cu, Fe, Mn), AlCuFe and (Al, Cu) Mn. The S-phase that occupied 2.7 per cent of the total surface area was active, leading to Mg and Al being selectively dissolved and leaving a pit at the particle location. S-phase dealloying also produced Cu-rich particle remnants that were cathodic to the matrix and therefore caused the peripheral formation of pits around the particle. It was also noted that some of the Cu-rich particles were decomposed into small mobile clusters and could be carried out from the pit, probably by mechanical action.

In another paper, Buchheit *et al.* [**21**] studied the localized corrosion behaviour of AA 2090.

Two types of pitting were found. The first was attributed to the dissolution of subgrain boundary phase T1 (Al_2CuLi), confirmed by the positive relationship between increased subgrain boundary precipitation and subgrain boundary pitting. The second type of pitting involved an enhanced local galvanic attack of the matrix material surrounding the AlCuFe constituents occurring randomly throughout the plate.

Many electrochemical studies of pitting corrosion have found characteristic potentials [**3**]. Using cyclic polarization techniques, two characteristic potentials can be determined corresponding to pit initiation and re-passivation. The observation and quantification of initial metastable pits are particularly important [**22**].

The interaction between corrosion and fatigue durability of aluminium alloy aircraft structures has been the subject of numerous investigations in recent decades. Much of this work has been motivated by situations when exploitation of aluminium alloys occurs under the corrosion-promoting conditions, such as salt-containing sea spray and vapour. Since these conditions are experienced by ship-based naval military aircraft, a considerable amount of research into the subject has been conducted and published by the Office of Naval Research in the US. In reference [**23**], the interaction between corrosive environment and mechanical overloads is explored. The authors conclude that the reduction of fatigue life occurred primarily due to corrosion pit formation, and also anodic dissolution at the crack tip accompanied by hydrogen embrittlement. This caused considerable acceleration of crack growth rates, particularly at low stresses, so that the endurance limit for the material could no longer be observed under these conditions. Collaborating academic laboratories have contributed to the development of test conditions representative of service environment [**24**] and investigation of the behaviour of specific aerospace aluminium

alloys [**25**, **26**]. The understanding of the mechanical integrity and fatigue durability in the presence of a corrosive environment gets incorporated into structural integrity and health monitoring models [**27**].

In the approaches found in the literature and reviewed above, only the relationship between the effect of an exposure to corrosive environment, on the one hand, and the consequences for overall structural integrity, on the other, was investigated. No attempt has been made so far, to the best of the authors' knowledge, to consider specifically the micromechanisms of corrosion, on the one hand, and the micro-mechanics of fatigue, on the other. The principal novel objective of the present investigation is an attempt to establish and verify the *connection* between *electrochemical* and *micro-mechanical* parameters of the near-surface layers, on the one hand, and residual fatigue lifetime, on the other. Despite the considerable volume of published work on the interaction between corrosion and fatigue, this connection does not figure prominently in the literature. A further novel aspect of the present work is the attempt to investigate these effects in test pieces that have experienced long-term, real service conditions. It is then possible to consider the possible reasons for such a connection and discuss the implications for lifetime estimation. To this end, it was decided to analyse coupons of polycrystalline aerospace alloys that were taken during repair from aircraft that to that point had experienced different fatigue loading histories, both in terms of the duration of exploitation and the number of flights made. Naturally, the availability of such samples is limited. In order to substantiate the findings made using coupons, test specimens were also prepared and subjected to laboratory experiments using electrochemical, mechanical and X-ray diffraction equipment.

The fundamental task of developing reliable physically based methods of residual fatigue lifetime assessment is formidable and could not be fulfilled entirely within the framework of the present research. Without aiming to provide conclusive answers, this paper presents some useful data on the observed connection, puts forward ideas about the specific microstructural mechanisms that may be responsible for this connection, and discusses how these ideas can be used to develop new modelling approaches. Deeper insight into the problem of fatigue–electrochemistry interaction is required to develop applications of electrochemical measurements for express fatigue monitoring.

2 EXPERIMENTAL

Coupons from the fuselage skin of Russian TU-154 airplanes were obtained from industrial inspection and repair units. All coupons were cut out from the section located between frames 53 and 66 (stringers 29-35-44). This zone of fuselage is subjected to the most severe cyclic loading during flights. Coupons 1, 2, and 3 corresponded to the airplanes that had 11, 15, and 20 years of exploitation, respectively. However, the intensity of their annual flight usage was different, at 565, 856, and 648 flights per year, resulting in a total of 6216, 12 834, and 12 953 flights, respectively.

A series of standard dog-bone specimens for laboratory cycling fatigue tests were prepared from as-supplied plates (see Fig. 1). The tests were conducted using a universal MTS servo-hydraulic testing machine in the cyclic fatigue tension loading regime with the maximal stress of 150 MPa, the R-ratio of 0.1, and the frequency of 10 Hz. Specimens were subjected to different maximum numbers of loading cycles varying in the range between 2500 and 50 000 cycles.

Aluminium alloy plates in the as-received condition had a cladding of unalloyed (99.9 per cent commercial purity) aluminium. In order to make the experiments representative of the alloy response, particularly in the tests where the response of the near-surface layers was crucial, the cladding was removed by chemical etching in 10 per cent NaOH at 65 °C with subsequent chemical brightening in 25 per cent HNO_3 for 2 s. Electrochemical tests were conducted in a purpose-built electrochemical analysis unit, built on the basis of the potentiostatic PI-50-1 set-up (Gomel Electrotechnical Company, USSR). Depending on the type of electrochemical test, 12 per cent H_2SO_4 or 3 per cent NaCl solutions were used for measuring electrochemical potentials or for potentiodynamic (voltamperometric) scanning.

The measurement of electrochemical potentials was conducted in an electrochemical analysis unit using a three-electrode circuit with specimens submerged into the electrolyte. Also, an accelerated 'drip' method was used, whereby a droplet of electrolyte is placed on the alloy surface with the help of a specially designed device.

Anodic polarization curves were obtained by the potentiodynamic method, following a preliminary cathode polarization treatment at a potential of 50 mV lower than the corrosion potential for the system. Potentiodynamic scanning was performed at a rate of

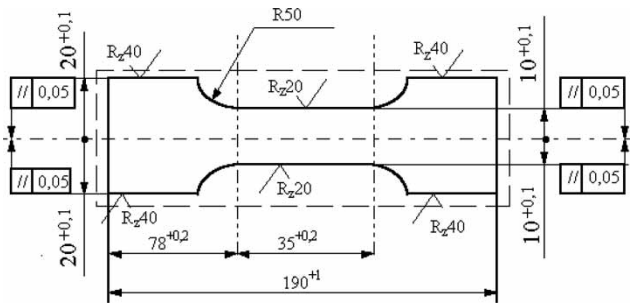

Fig. 1 Design of the specimen used for monotonic and cyclic tensile testing

2 mV/s up to the maximum value of +0.6 to +0.8 V. Susceptibility to pitting corrosion was evaluated using the galvanostatic method [**27**].

Light microscopy studies were carried out using a NEOPHOT-2 microscope (Carl Zeiss, Jena, DDR) at 100×, 250×, and 500× magnification to investigate the structure in cross-section fields both in undamaged and corroded sites, under layers of general corrosion products and in the vicinity of a corrosion pit. Scanning electron microscopy (SEM) investigations were performed at 400× and 1000× magnification using a JSM-35CF microscope (JEOL, Japan) with chemical analysis attachment. The characteristic depth of microchemical analysis was about 10 μm in the present experiments.

X-ray diffraction analysis was conducted using a computer-operated diffractometer DRON4 (Burevestnik, St Petersburg, Russia) in step-scanning mode. Co-Kα, Ni-Kα, Cu-Kα, and Mo-Kα radiations were used in symmetric Bragg–Brentano geometry with a graphite secondary monochromator. The acquired X-ray diffraction patterns were analysed using an in-house computer software package [**28**]. The study of the crystallographic texture and lattice defect structure was carried out by considering the 111, 200, 220, and 311 peak intensities and profiles.

Transmission electron microscopy (TEM) investigations of the microstructure were conducted using a JEM-200CX microscope (JEOL, Japan) at 160 kV, which provided a satisfactory spatial resolution for 20 000× and 100 000× magnification. Several (10–15) thin foils were prepared from the bulk of plate specimens for all the cases studied, and 50–60 fields were looked through for each foil and magnification.

Chemical composition in the thin surface layers (10–100 nm thick) was investigated by means of secondary ion mass spectroscopy (SIMS). The computer-operated mass spectrometer MS7201M (Russia), which combines a vacuum system (no worse than 5×10^{-6} Pa), an Ar^+ ion gun (ion energy $E =$ 4.5 keV and operating current density 20–30 mA/cm^2) and a registration system, was capable of analysing an approximately 5 nm-thick layer over an area of 1 cm^2. The profiles of element distribution through sample depth were obtained during *in situ* ion etching (the etching rate was about 5 nm/min). The accuracy of the secondary ion current density measurement was no worse than 2–4 per cent of the measured value.

3 EXPERIMENTAL RESULTS AND DISCUSSION

3.1 Corrosion and performance

The aluminium alloy D16AT (3.8–4.9 per cent Cu, 1.2–1.8 per cent Mg, 0.3–0.9 per cent Mn, 0.5 per cent Fe, solution heat treated at 550 °C, cold water quenched, and naturally aged at room temperature) is the Russian equivalent of the alloy 2024-T4, which typically contains 4.4 per cent Cu, 1.5 per cent Mg, and 0.6 per cent Mn and undergoes a similar solution heat treatment. Structural components made from this alloy experience various corrosion effects during service in aviation. Examples of corrosion damage are shown in Fig. 2.

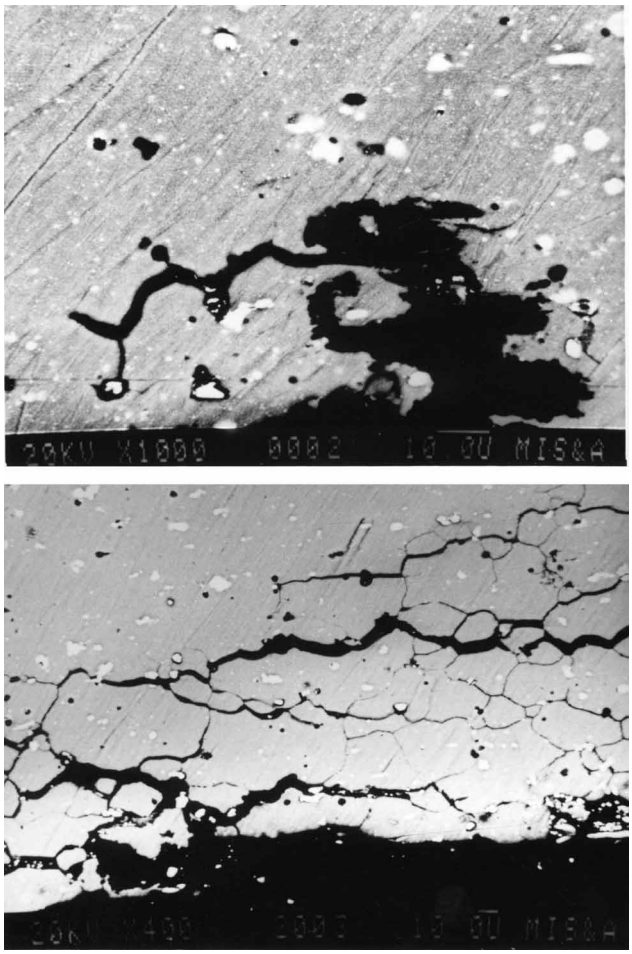

Fig. 2 (a) Pitting corrosion in the alloy after 11 years of exploitation. (b) Intercrystalline corrosion in the alloy after 20 years of exploitation

Visual examination of fuselage skin fragments reveals that the plates show evidence of significant corrosion mainly on the internal (concave) surface of the plate (Fig. 2). This is likely to be associated with the fact that condensation of atmospheric moisture responsible for causing corrosion occurs on the inner side of fuselage skin. Exploitation procedures do not prescribe any special protective coatings or drying procedures for this surface.

Unequal amounts of corrosion were found in the fragments investigated. Some sites were completely free from signs of corrosion, and traces of initial varnish and clad coating could be clearly distinguished. Other sites were more or less severely corroded, showing some various levels and types of corrosion damage, from spots to pits.

It was found that the degree of corrosion (the ratio of the corroded surface area to the entire area) was not a direct function of exploitation time. Up to 30 per cent of the alloy surface was affected by general non-uniform corrosion in the fragments after 11 years of exploitation, up to 40 per cent of the fragment surface for fragments after 15 years of exploitation, while in coupons having had 20 years of exploitation only 25 per cent of the fragment surface was corroded. This fact shows that operating time on its own cannot serve as a criterion for the estimation of safe residual lifetime under the conditions of corrosion. The degree of corrosion appears to be rather specific to an airplane, the weakest degree of corrosion corresponding to the longest operating time. The degree of corrosion is likely to depend mainly on the exposure conditions during service, i.e. the characteristic moisture–temperature regime at airports and on the routes where a particular airplane is exploited. For example, sea climate is more likely to cause significant corrosion, because of the higher content of active ions from sea water in the atmosphere.

It has been observed that corrosion damage tends to be non-uniform in terms of its depth over the fragment surface of fuselage skin boards. The maximum depth of corrosion pits in the fragment was about 0.4 mm after 11 years of exploitation, 0.9 mm after 15 years, and 1.1 mm that after 20 years. Therefore, in contrast with the degree of corrosion, the maximum depth of corrosion increased steadily with the operating time. This suggests that localized types of corrosion become dominant under long-term exploitation conditions.

In order to estimate the susceptibility to pitting of the uncorroded alloy after different operating times, the pitting potential, E_P, was measured by the galvanostatic method [**29**]. The data on E_P for all alloys studied are presented in Table 1.

The values of ΔE_P obtained give evidence that fuselage skin fragments after 11 years of exploitation exhibit the minimum susceptibility to pitting, while those after 20 years have maximum susceptibility. It is also apparent that the value of ΔE_P after 15 years of exploitation is much closer to that after 20 years of exploitation, suggesting that the alloy in these conditions has similar corrosion behaviour and susceptibility to pitting. It can be noted generally that the difference between the corrosion potential and the pitting potential tends to decrease and eventually vanish with increasing operating time, indicating that longer operation enhances localized corrosion modes, e.g. pitting. However, light microscopy studies reveal that, in accordance with published reports [**30**], other types of local corrosion (intercrystalline corrosion (ICC) and layer corrosion (LC)) are also found, resulting in non-uniform corrosion over the material's surface [**31**].

Table 1 Pitting potential of D16AT alloy after various operating times (galvanostatic method, 3% NaCl solution, current density $i = 0.17$ mA/cm^2)

Operating time (years)	Corrosion potential E_C (V)	Pitting potential E_P (V)	$\Delta E_P = E_P - E_C$ (V)
11	−0.372	−0.323	0.049
15	−0.357	−0.333	0.024
20	−0.353	−0.347	0.006

The alloy after 11 years of exploitation is subjected to both general non-uniform corrosion and local corrosion of one dominant type, namely, pitting (see Fig. 2(a)). In the alloy after 15 years of exploitation alongside the pitting described above, pronounced ICC extending to a depth of 200 μm was also detected (the overall appearance is shown in Fig. 3). It is interesting to note that traces of ICC are only found around some isolated pits, but are not visible at the sites affected by general corrosion. This observation suggests that ICC may be a result of pitting evolution.

The alloy after 20 years of exploitation also shows the presence of pitting and traces of ICC (see Fig. 2(b)). The depth of ICC propagation does not exceed the level reached in the alloy after 15 years of exploitation. However, in the alloy after 20 years of exploitation, sites damaged by LC were also detected.

As a consequence of non-uniform corrosion (especially due to local corrosion), fracture of material under normal operating loadings becomes possible. This has been confirmed in a series of tensile tests. The presence of corrosion damage in the specimens results in the reduction of mechanical properties after 15 and 20 years of exploitation, namely strength and ductility (see Table 2).

It is clearly seen from Table 2 that for the alloy affected by pitting corrosion alone after 11 years of exploitation, only ductility is significantly reduced. For the alloy showing signs of both pitting and ICC after 15

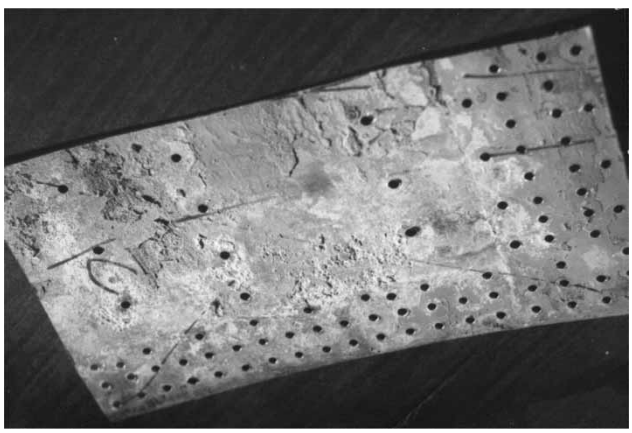

Fig. 3 General appearance of corrosion in a fuselage panel after 15 years of exploitation

Table 2 Mechanical properties of the corroded aluminium alloy D16AT

Operating time (years)	Yield stress, $\sigma_{0.2}$ (MPa)		Tensile strength, σ_B (MPa)		Elongation to fracture, δ (%)	
	No corrosion damage	With corrosion damage	No corrosion damage	With corrosion damage	No corrosion damage	With corrosion damage
11	348.0 ± 5.6	357.9 ± 5.9	463.3 ± 4.3	475.8 ± 5.5	14.3 ± 0.8	11.4 ± 3.2
15	385.0 ± 11.1	367.7 ± 3.7	495.6 ± 16.5	460.4 ± 25.0	13.0 ± 2.1	9.8 ± 3.8
20	363.4 ± 10.1	358.2 ± 5.9	473.9 ± 6.5	445.0 ± 15.7	14.6 ± 2.7	8.2 ± 1.7

years of exploitation, both the strength characteristics and ductility were reduced. The most significant reduction of ductility was found in the alloy after 20 years of exploitation, which is affected by general non-uniform corrosion and all types of local corrosion. The reduced mechanical performance in this case is also expressed in the decrease of yield stress and ultimate strength.

It was further established that the removal of corrosive damage (spots and pits) by mechanical grinding results in a practically complete recovery of the mechanical characteristics. However, in the cases where some corrosion pits remained after grinding, the effect of mechanical property degradation was preserved. Table 3 demonstrates this statement for the alloy after 15 years of exploitation.

It was also found in fatigue tests that general uniform corrosion (to a depth of up to 20 per cent of the specimen thickness) results in a five- to eight-fold reduction in the specimen lifetime (measured to the point of crack initiation). The presence of LC damage to the depth of up to 15 per cent of the specimen thickness decreases the specimen lifetime by six to eight times. General corrosion (even in the absence of spots and pits) also increases the rate of fatigue crack growth. Crack length measurements were made as a function of the number of cycles for both uncorroded and corroded samples (six and nine samples in each case, respectively). After data reduction (Paris logarithmic linearization) it was established that the rate of fatigue crack growth in corroded samples is about 1.4 times greater than in the uncorroded samples. The influence of corrosion on fatigue crack initiation is also discussed below.

Table 3 Mechanical properties of corroded and mechanically ground aluminium alloys D16AT (after 15 years of exploitation)

Corrosion damage level	Yield stress, $\sigma_{0.2}$ (MPa)	Tensile strength, σ_B (MPa)	Elongation to fracture, δ (%)
Uncorroded	385.0 ± 11.1	495.6 ± 16.5	13.0 ± 2.1
Corroded (general corrosion)	357.9 ± 5.9	460.4 ± 25.0	9.8 ± 3.8
Mechanically grind (corrosion spots and pits removed)	387.0 ± 8.9	496.5 ± 7.0	11.8 ± 2.1
Mechanically grind (corrosion pits remained)	376.6 ± 7.8	458.0 ± 21.8	6.8 ± 2.5

It is recalled that the analysis of corrosion and mechanical properties of aluminium alloy D16AT coupons shows that operating time alone cannot be used as a reliable basis for the estimation of corrosion damage and performance reduction. The interaction between microstructural changes induced by fatigue and corrosion is likely to have a complex character, and must be studied systematically in specially prepared laboratory test specimens.

3.2 The change of mechanical properties with operating time

The data on the evolution of mechanical properties during operating time are given in Table 4 for specimens without any traces of corrosion.

Mechanical properties appear to reach a peak and start to decrease (see Figs 4(a) and (b)) if these properties are plotted against operating time. This may suggest the presence of competing mechanisms for structural change. However, if mechanical properties are plotted versus flight intensity, i.e. the number of flights per year (see Figs 4(c) and (d)), then the trend observed is closer to a monotonous variation. Statistical analysis shows that the hypothesis of the statistical significance of mechanical property difference in all the states investigated can be accepted with 98 per cent reliability. It is concluded that the evolution of mechanical properties is caused by structural changes. Assuming that these structural changes are induced by fatigue, the following two possible causes are discussed further in this study.

1. Cyclic fatigue loading leads to the generation of new lattice defects and promotes the rearrangement of existing lattice defects into stable structures (mainly dislocation ladders, cells, walls, persistent slip bands, etc.).
2. Cyclic fatigue loading affects the process of ageing, i.e. decomposition of supersaturated solid solution, precipitate formation, loss of coherence and growth, and interaction with lattice slip.

TEM studies reveal no significant difference in the structural state of the alloy at all operating times. The

Table 4 Mechanical properties of uncorroded aluminium alloy D16AT coupons after different periods of exploitation. Minimal mechanical properties of Alclad 2024-T4 alloy (UNS number A92024): tensile strength 450 MPa, yield strength (0.2%) 295 MPa, and elongation to failure 19%

Operating time (years)		Yield stress, $\sigma_{0.2}$ (MPa)	Tensile strength, σ_B (MPa)	Elongation to fracture, δ (%)
As supplied	Minimal guaranteed	275–280	415–435	11–13
	Typical at 20 °C	290	440	19
	From statistical distribution	305 ± 10	450 ± 10	17 ± 2
11		347.98 ± 5.57	463.32 ± 4.26	14.27 ± 0.86
15		385.03 ± 11.13	495.62 ± 16.46	12.97 ± 2.12
20		363.43 ± 10.09	473.92 ± 6.52	14.59 ± 2.70

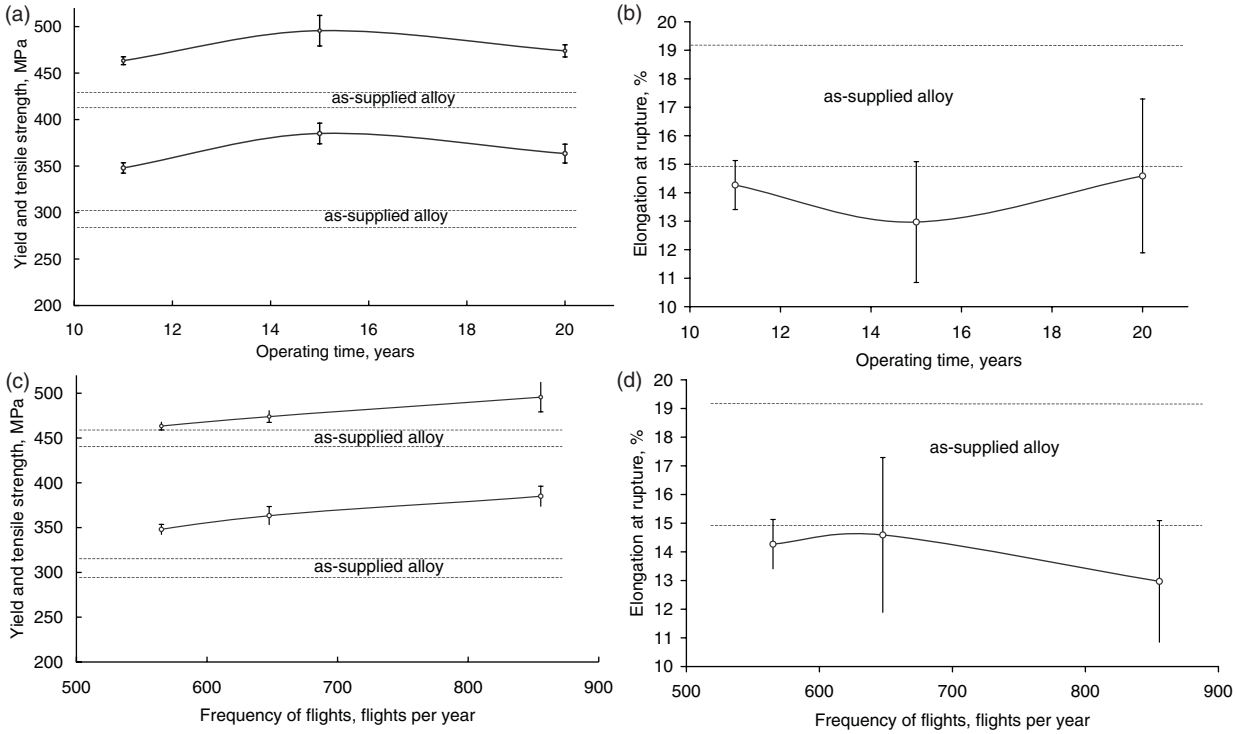

Fig. 4 Evolution of mechanical properties during service: (a) yield and tensile strength versus operating time in years; (b) ductility versus operating time in years; (c) yield and tensile strength versus frequency of flights; and (d) ductility versus frequency of flights

structure of alloys in the plane parallel to the surface of the plate has several common features. They are as follows.

1. Equiaxed grains are of 20–30 μm diameter, with a dominant orientation of the crystallographic (100) plane coplanar to the plate specimen surface.
2. Lamellar oval particles (of 0.2 μm main diameter on average) are almost randomly distributed in the matrix. These are particles of the Al–Fe or Al–Mn intermetallics, arising due to the unavoidable technological contamination of the alloy with Fe and Mn impurities during manufacture.
3. Randomly distributed dislocations have low scalar density (10^8–10^9 cm^{-2}). Significant numbers of helical dislocations are noticeable, which is evidence for the presence of sinks of quenched vacancies. Some edge dislocation loops (vacancy discs) were also visible in the TEM images.
4. Selected area electron diffraction (SAED) images reveal the presence of randomly distributed Guinier–Preston zones (crossed diffuse lines are visible in the SAED images in Fig. 5).

The observations in this study suggest that low-stress, high-cycle fatigue during operating time causes no dramatical structure changes in the bulk material. Neither phase composition and microchemical inhomogeniety, on the one hand, nor lattice defect density and dislocation structure, on the other, evolve to a significant degree. This phenomenon is widely discussed in the literature [**32**] for high-cycle fatigue. It is generally accepted that fatigue failure is the result of microcrack growth. However, the precise nature

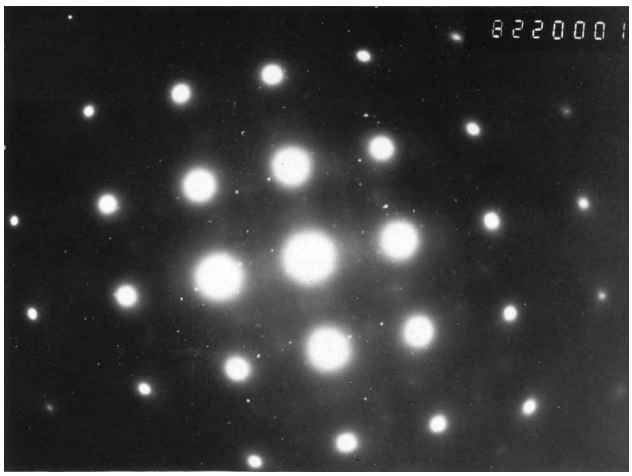

Fig. 5 SAED image taken from a grain with typical (100) orientation, showing the crossed line pattern from the Guinier–Preston zones

of a microcrack initiation is mostly not identified in sufficient detail for various alloy systems. At the specimen surface, the stresses under external loading are often concentrated because of specimen design (e.g. notches or holes) or surface roughness (scratches and pitting). The near-surface region is the likely location for microcrack initiation, even when such microcracks were not inherited or introduced by a reason other than fatigue. As demonstrated above, general corrosion effects, and especially layer and intercrystalline corrosion, are significant factors causing a decrease of the lifetime, since corrosion damage produces ready sites for microcrack initiation.

TEM analysis elucidates the mechanism of intercrystalline corrosion in the D16AT aluminium alloy. The presence of helical dislocations and vacancy loops indicates that these lattice defects act as fast sinks for the quenched vacancies. Grain boundaries are also likely to act as fast sinks. Therefore, regions of alloy close to grain boundaries tend to become depleted of vacancies, and diffusion in these regions becomes suppressed. This slows down the decomposition of the supersaturated solid solution, leaving the grain boundaries supersaturated, mainly in the more electropositive Cu. Hence, grain boundaries themselves become particularly prone to corrosion.

Finally, TEM studies of samples taken from alloy bulk allowed one to reject both hypotheses put forward above for the mechanisms responsible for changing mechanical properties. It is found that fatigue modifies neither the dislocation structure nor the ageing process in the bulk of the D16AT alloy. Establishing this negative answer to the questions posed above necessarily requires one to focus on the structural changes in the near-surface layers of the material. Evidently, it is the structural state of the near-surface layer that affects the mechanical properties to a serious extent [**33**]. As a consequence of this conclusion, further analysis is focused on the surface-sensitive methods of electrochemical testing and X-ray diffraction.

3.3 Structural state in the surface layer

In order to investigate the influence of fatigue on the structure of the near-surface regions, stepwise layer-by-layer etching was conducted, and X-ray diffraction and electrochemical tests were carried out [**34**]. The results of these experiments are given in Figs 8 to 13.

Both techniques show the existence of a transition layer, where dramatic changes occur both in the electrochemical corrosion potential, and in the diffraction pattern parameters, such as the polar density and physical broadening of different X-ray reflections. This transition layer is likely to correspond to the interface between the cladding and the base plate alloy.

Crystallographic texture dominated by the (110) plane lying in the plane of the specimen is found in the cladding and is typical of cold rolling, while a texture characteristic of recrystallization after rolling (preferred orientation of the (100) plane in the plane of the specimen) was found in the bulk alloy. This combination arises at the final technological step in the production of D16AT, when the alloy plate after main rolling and quenching from 550 °C is gently rolled together with a pure aluminium foil, the material used for cladding. The data on crystallographic texture of the bulk of the alloy were obtained by TEM and found to be in perfect agreement with the data from X-ray diffraction analysis for the deepest layer analysed.

The recorded values of X-ray peak broadening were close to the lower limit of sensitivity for dislocation density evaluation, i.e. all X-ray peaks were quite narrow. The estimation of dislocation density by the physical broadening of the 311 line gives the value of the order of 10^9–10^{10} cm^{-2}, which differs from the value estimated in TEM studies. It is suggested that substitutional atoms of species other than Al present in the supersaturated solid solution cause additional statistical displacement of the scattering atoms, thereby making an additional contribution to X-ray peak broadening.

The electrochemical potential varies for different crystallography planes and its gradual increase occurs in the sequence (100)→(110)→(111) [**35**]. Thus a decrease of electrochemical potential with depth should be expected for the clad D16AT alloy, assuming that this potential is modified by texture alone. Another cause of electrochemical potential variation may be the change in the dislocation density. However, if the rise in physical broadening with depth is related to the higher dislocation density alone, this would lead to the more negative electrochemical potential of corrosion. The present experimental data contradict both the tendencies discussed above, suggesting that the increase of corrosion potential with depth must be

related to the change in chemical composition, i.e. the higher content of the more electropositive elements in the alloy.

The dependencies of the polar density and X-ray peak breadth on operating time are ambiguous. Provided that the change of polar density does not reflect the sample-to-sample variation, one may conclude that the polar density of the (110) planes gradually decreases with operating time in both the near-surface and deep layers of the material, while the polar density of the (100) planes seems to increase with the frequency of flights. Peak broadening tends to increase with operating time in the case of deep layers and with the frequency of flights in the case of surface layers.

Electrochemical tests characterize much thinner layers of material than conventional laboratory X-ray diffraction analysis. By the choice of X-ray radiation source from the range between Co-Kα and Mo-Kα, the penetration depth into Al can be changed from about 50 to 750 μm. In comparison, during potentiodynamic scanning, only 0.05–0.1 μm is dissolved at the maximum current density used (1 μA/cm^2). Thus electrochemical tests may be preferred for the investigation of fine effects in the transition layer. The data of electrochemical tests can be compared with those from SIMS.

It has been found that, while the evolution of X-ray characteristics with depth is rather smooth, the dependence of corrosion potential on depth shows some peculiarities. After the rise of potential in the transition layer, some characteristic minimum of potential is observed at a certain depth for the alloys after 11 and 20 years of exploitation. It is suggested that the same dependence is likely to be valid for the alloy after 15 years of exploitation. However, only part of the complete curve was obtained in the present experiments. Moreover, there exists a dependence of the character of the anodic polarization curve on depth. In Fig. 6 anodic polarization curves are shown for different depths. Only weak general anodic dissolution is detected with no distinct peaks in the surface layer, while at a certain depth intensive anodic dissolution with several distinct peaks is present. The last effect tends to be weaker in the deeper layers of material.

Microchemical analysis reveals some important trends affecting the corrosion behaviour of the D16AT alloy. First, SEM investigation of alloy surface after potentiodynamic scanning where distinct peaks were observed reveals no difference in the content of all components expect Fe. For Fe, however, the content in the test region is 50 per cent lower in comparison with the untested zone. This fact probably indicated selective dissolution of the Al–Fe intermetallic particles during testing. Accelerated pitting in the vicinity of Fe-rich phases in Al-based alloys was also reported in reference [**36**].

Second, in SIMS experiments the current of Cu and Mn secondary ions tends to be two to three times higher in the surface layer than in deep layers (see Fig. 7), while the current of Al and Mg secondary ions tends to be lower in the surface layer than in the deep layers. This chemical inhomogeneity is likely to be the reason for higher corrosion resistance of the surface layers. It is also believed that the variation of potential

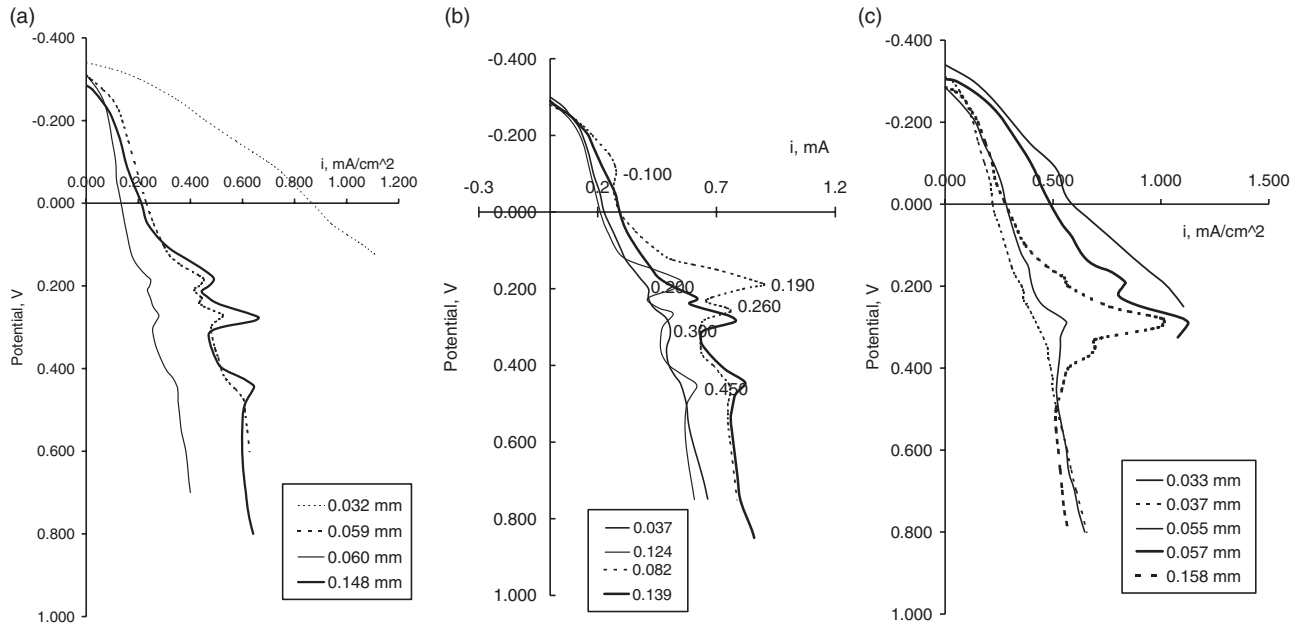

Fig. 6 The evolution of the anodic polarization curve shape for different depths in the alloy (shown in the legend) after: (a) 11 years of exploitation, (b) 15 years of exploitation, and (c) 20 years of exploitation

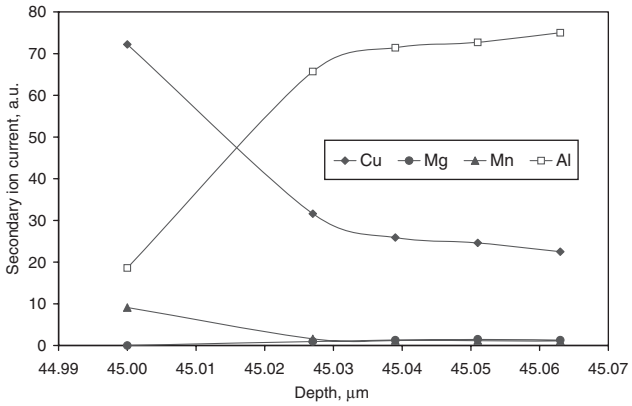

Fig. 7 A typical result of SIMS analysis showing the element distribution with depth in the alloy after 15 years of exploitation (below the clad coating)

with depth is related to the chemical inhomogeneity in the surface layers of material.

It is concluded that the dependence of the corrosion potential in the near-surface and deep layers on the operating time is complex. Several outstanding questions remain. First, is chemical inhomogeneity induced by fatigue? Second, if so, then what is the mechanism for the generation of this chemical inhomogeneity? Third, is it possible to use the effect of chemical inhomogeneity induced by fatigue for the prediction of safe remaining lifetime? Analysis of these problems is the subject of the final part of the present report. Laboratory fatigue tests were used in order to impose well-specified fatigue conditions and minimize sample-to-sample variation, and detailed characterization by electrochemical and X-ray diffraction analysis was carried out.

The evolution of structure in the surface layers of alloy during fatigue cycling tests: two sample preparation techniques were used in order to investigate the influence of fatigue on the electrochemical and X-ray characteristics of the alloy surface layers.

1. A series of 60 identical specimens of standard shape were cut from a single as-supplied plate of the D16AT alloy. The specimens were subjected to fatigue cycle loading with various numbers of cycles. Then cladding coating was removed by etching and almost identical thinning was obtained for all specimens.
2. Cladding coating was removed by etching from several specimens. Every specimen was characterized after each portion of fatigue cycle loading and these results were accumulated until the specimen's failure.

The results of experiments using technique 1 are shown in Figs 8 to 12. The accelerated droplet method reveals no definite trend in the dependence on the number of cycles of the electrochemical potential at

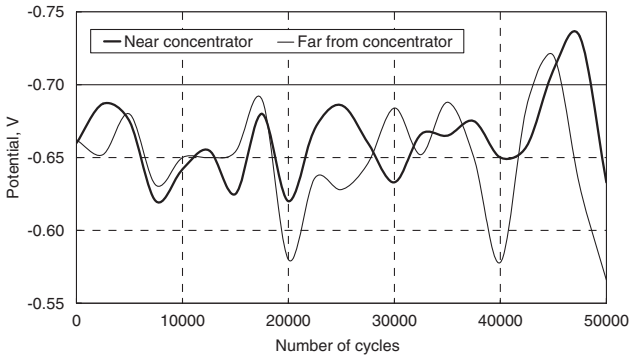

Fig. 8 The evolution with the number of cycles of the electrochemical potential (3 per cent NaCl) in the clad coating of D16AT alloy subjected to laboratory fatigue testing

the clad surface (Fig. 8). The same random variation was revealed when X-ray characteristics (polar density in Fig. 9 and physical broadening in Fig. 10) were considered for the clad surface. These observations

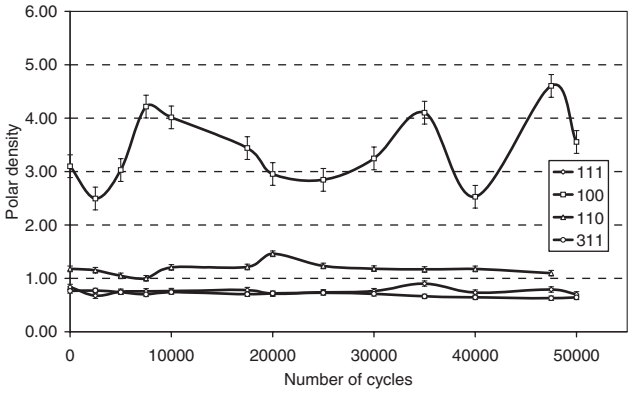

Fig. 9 The evolution with the number of cycles of the polar density in the clad-free surface of D16AT alloy subjected to laboratory fatigue testing

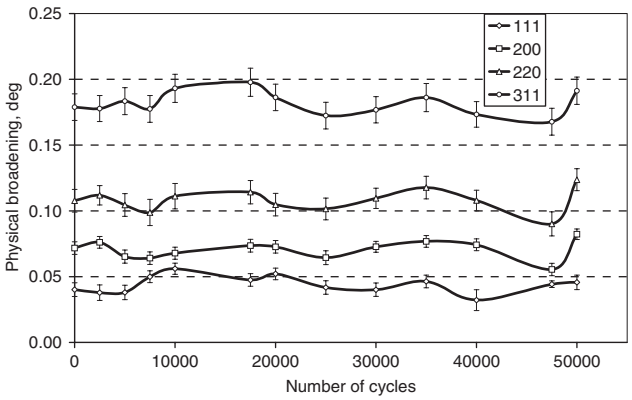

Fig. 10 The evolution with the number of cycles of the physical broadening in the clad-free surface of D16AT alloy subjected to laboratory fatigue testing

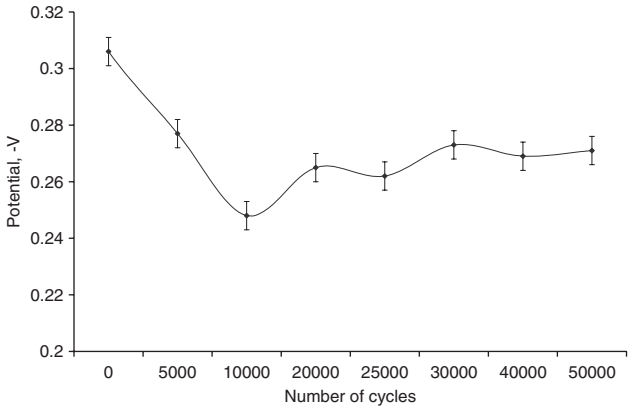

Fig. 11 The evolution with the number of cycles of the corrosion potential (12 per cent H_2SO_4) in the clad-free surface of D16AT alloy subjected to laboratory fatigue testing

correspond to the conventional paradigm of high-cycle fatigue, where no clearly discernible structural changes are thought to occur in the sample.

However, different trends were observed at the clad-free alloy surface. The corrosion potential reaches a maximum after 10 000 cycles and eventually approaches a steady-state level after 30 000 cycles. A general increase of potential with the number of cycles is detected, which is ascribed here to the increasing chemical inhomogeneity induced by fatigue. This may be due to layers of alloy lying at certain depths tending to become enriched in the more noble elements. It is also apparent from Fig. 12 that fatigue affects the form of the anodic dissolution curve obtained during potentiodynamic scanning.

Other trends are found for the surface layers of samples prepared using technique 2. First, the corrosion potential generally tends to decrease with the number of cycles both in the vicinity and far from the round concentrator hole machined in the specimens. However, a transient maximum of potential could be detected at an early stage of cycling (Fig. 13). Second, physical broadening increases rapidly in the earliest period of specimen's cyclic life, and remains largely constant for the remaining lifetime (Fig. 14). The increase in the physical broadening is more pronounced near the concentrator. In the narrow zone near a growing crack the value of physical broadening may differ from that in the larger zone around the concentrator. This phenomenon is ascribed here to a complex character of structural evolution near the

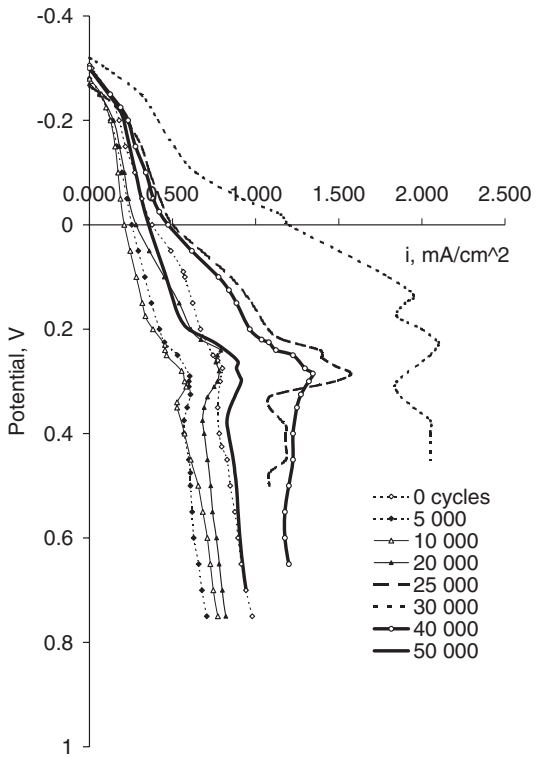

Fig. 12 The evolution with the number of cycles of the potentiodynamic anodic polarization curves in the clad-free surface of D16AT alloy subjected to laboratory fatigue testing

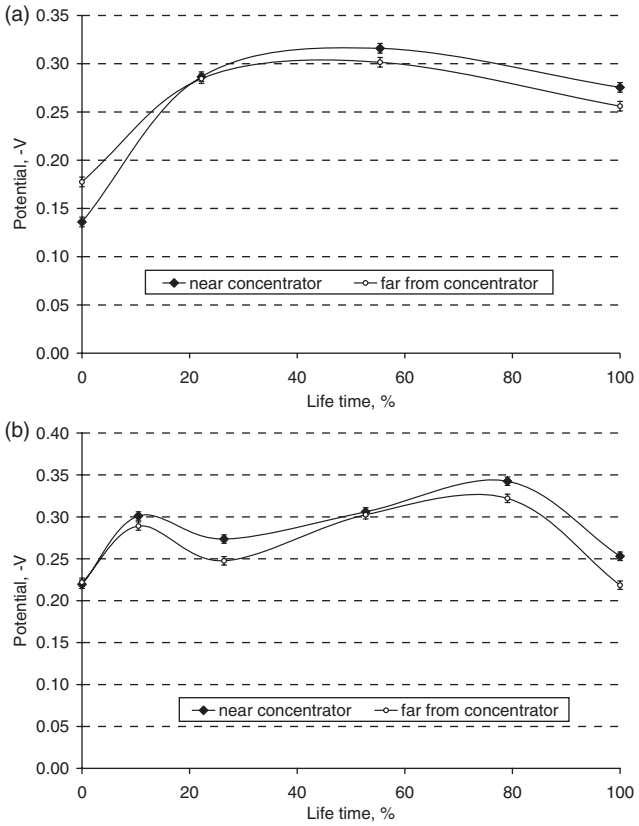

Fig. 13 The evolution of corrosion potential (10 per cent H_2SO_4, the 'drip' method) during the life of a single specimen subjected to a fatigue test. Measurements were taken in the vicinity of and away from: (a) a small round concentrator and (b) a large round concentrator

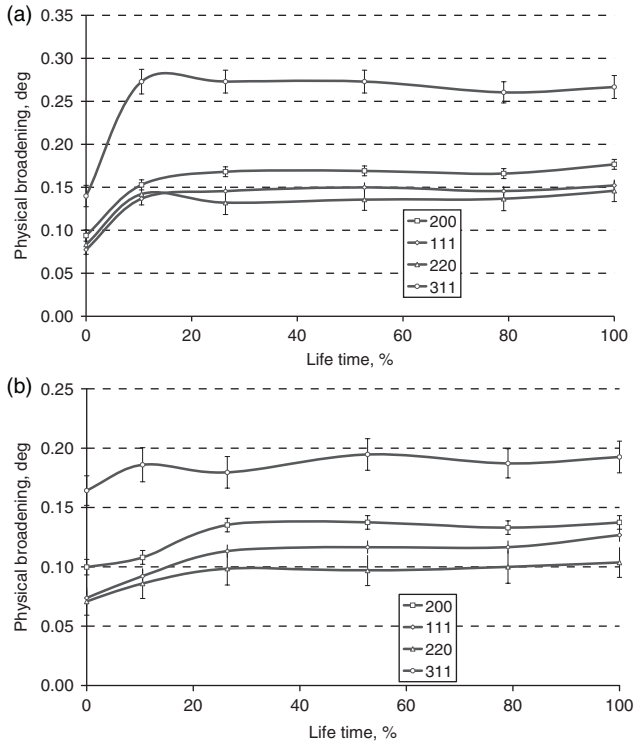

Fig. 14 The evolution of X-ray peak physical broadening during the life of a single specimen subjected to a fatigue test. Measurements were taken: (a) in the vicinity of and (b) away from a small round concentrator

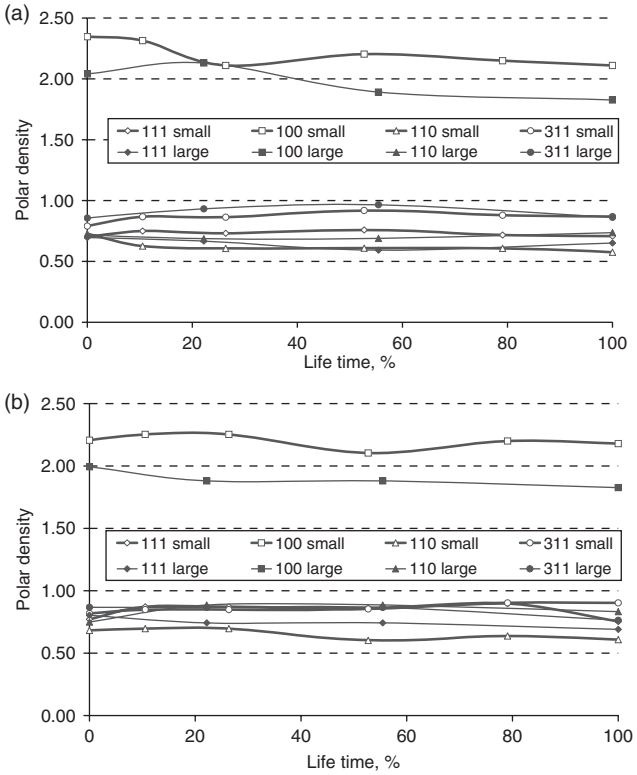

Fig. 15 The evolution X-ray peak polar density during the life of a single specimen subjected to a fatigue test. Measurements were taken: (a) in the vicinity of and (b) away from a small round stress concentrator and a large round stress concentrator (as indicated)

faces of the crack, since local severe plastic deformation and possible contact between crack shores may induce additional local heating and transformations. Finally, no changes of crystallographic plane polar densities were observed (Fig. 15).

Contradictory tendencies of corrosion potential evolution in the surface layers of the D16AT alloy samples were found, which are likely to be related to the different ways of sample preparation. Since the increase of physical broadening for pure alloy surface is accompanied by the decrease of potential, it is suggested that the increase of defect density (dislocations and dislocation pile-ups, microcracks and microscopic surface intrusions and extrusions) is the main factor reducing the potential. Thus the effect of fatigue-induced inhomogeneity is masked. On the other hand, if the cladding is present, the lattice defects become concentrated mainly in this coating, so that the effect of induced chemical inhomogeneity in the base alloy surface can be observed.

4 DISCUSSION

On the basis of the extensive experimental investigation described here, it can be concluded that, for the aluminium alloy investigated, both electrochemical and mechanical characteristics show steep variation in the near-surface region. By way of discussion and conclusion of the above results, here some suggestions about the cause of this variation of electrochemical (and hence mechanical) characteristics with depth are put forwarded.

A model is proposed, which is illustrated in Fig. 16. It is well known that during repeated reverse mechanical loading, plastic deformation (mediated by crystal slip) becomes concentrated in the thin near-surface layer. High-cycle fatigue gives rise to surface microroughness through the mechanisms of intrusions and extrusions, thus forming notch-like surface shapes that act as numerous micro-crack precursors in the surface. These defects also represent locations for easy fracture of the oxide film, thus stimulating the process of further oxidation. Al and Mg, the elements with the highest chemical affinity for oxygen, diffuse towards these sites, creating a gradient of chemical composition and electrochemical potential in the fatigued specimen. As a consequence of this accelerated diffusion and oxidation, the more noble Cu species accumulates in the surface layers.

The benefit of the view on fatigue electromechanics that is promulgated here and illustrated in Fig. 16

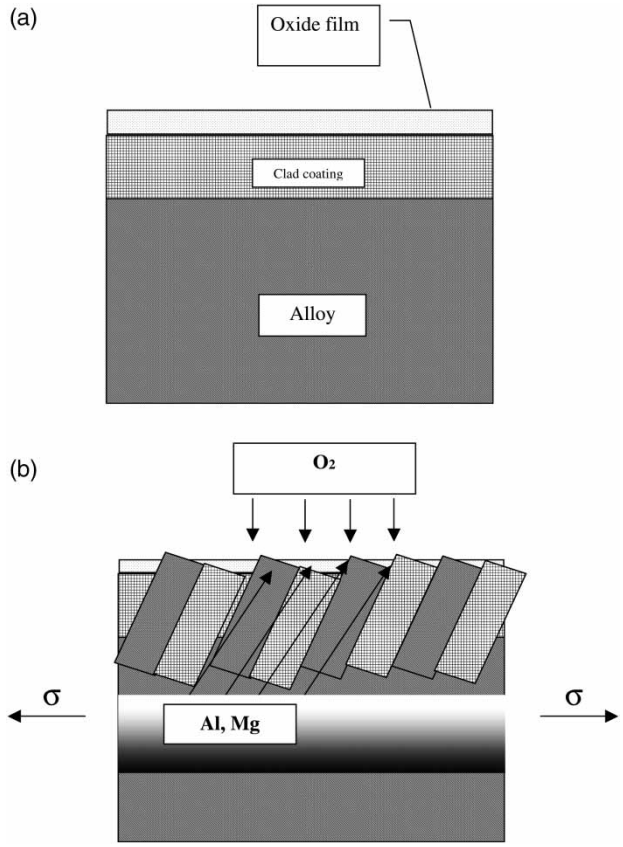

Fig. 16 An illustration for the mechanism of fatigue-induced chemical inhomogeneity: (a) initial structure of the clad alloy and (b) evolution of element concentration induced by fatigue

is that it highlights the clear link existing between mechanical deformation effects (slip, plasticity, and surface roughening) and chemical processes (surface oxide layer formation and break-up, and diffusion of alloying elements through the near-surface layers of the material). It is the authors' belief that this represents an improvement in the knowledge about the chemo-mechanics of fatigue in aluminium alloys.

5 CONCLUSIONS

In the present study, a variety of experimental techniques were employed to consider the complex interactions between fatigue and corrosion processes. The particular novelty of the present approach lies in the attempt to establish a *connection* between *electrochemical* and *micro-mechanical* properties of aluminium alloy samples and engineering components. A further substantial difference between the present study and others found in the literature is that real components that had experienced many years of service exposure were studied alongside laboratory test specimens.

Some experimental facts reported in the present study give evidence that changes in the structure and chemical composition during high-cycle fatigue of the aluminium alloy D16AT are confined to a very thin surface layer. It has been demonstrated that electrochemical tests are more sensitive to these changes than X-ray diffractometry.

Figure 11 illustrates the evolution with the number of cycles of the corrosion potential (12 per cent H_2SO_4) in the clad-free surface of D16AT alloy subjected to laboratory fatigue testing. A connection is observed between the corrosion potential and the number of cycles experienced by the material. After about 10 000 cycles the corrosion potential exhibits a reduction of about 30 per cent with respect to the initial value, followed by the gradual increase to a steady-state value that is about 20 per cent lower than the initial value. Note that structural changes in the aluminium alloy due to high-cycle fatigue loading are otherwise very difficult to detect.

Although certain difficulties were encountered both in the sample preparation and in the interpretation of experimental data, the data collected suggest that, in the longer term, further development of the electrochemical technique for fatigue diagnostics is likely to yield a useful and powerful means for safe residual lifetime evaluation. Finally, another novel development appearing in the present article is the newly proposed micro-mechanical model of the corrosion process, illustrated in Fig. 16.

Some mechano-chemical connection of the type sought has been established, although the results remain incomplete, and further investigations are clearly required.

REFERENCES

1 **Suresh, S.** *Fatigue of materials*, 1991 (Cambridge University Press, Cambridge).
2 **Vasiliev, V. Y.** and **Shapkin, V. S.** *Structural corrosion and electrochemical diagnostics of alloys*, 1998 (Russian Process Engineering Publishers, Moscow).
3 **Rao, K. S.** and **Rao, K. P.** Pitting corrosion of heat-treatable aluminium alloys and welds: a review. *Trans. Indian Inst. Met.*, 2004, **57**, 593–610.
4 **Uhlig, H. H.** Adsorbed and reaction-product films on metals. *J. Electrochem. Soc.*, 1950, **97**, 215.
5 **Sato, N.** Theory for breakdown of anodic oxide films on metals. *Electrochim. Acta*, 1971, **16**, 1683.
6 **Urquidi, M.** and **MacDonald, D. D.** *J. Electrochem. Soc.*, 1985, **132**, 555.
7 **Williams, D. E., Westcott, C.,** and **Fleischmann, M.** Stochastic models of pitting corrosion of stainless steels. *J. Electrochem. Soc.*, 1985, **132**, 1804.
8 **Foley, R. T.** Localized corrosion of aluminum alloys – a review. *Corrosion*, 1986, **42**, 277.

9 **Szklarska-Smialowska, Z.** Pitting corrosion of aluminium. *Corros. Sci.*, 1999, **41**, 1743–1767.

10 **Frankel, G. S., Stockert, L., Hunkeler, F.,** and **Bohni, H.** Metastable pitting of stainless-steel. *Corrosion*, 1987, **43**, 429–436.

11 **Szklarska-Smialowska, Z.** *Pitting corrosion of metals*, 1986, p. 347 (National Association of Corrosion Engineers (NACE), Houston, Texas).

12 **Godard, H. P.** The corrosion behavior of aluminum in natural waters. *Can. J. Chem. Eng.*, 1960, **21**(167), 104.

13 **Hunkeler, F.** and **Boehni, H.** Determination of pit growth rates on aluminum using a metal foil technique. *Corrosion*, 1981, **37**, 645.

14 **Dix, J. R., Brown, R. H.,** and **Binger, W. H.** The resistance of aluminum alloys to corrosion. In *Metals handbook 1*, 1975, p. 916 (American Society for Metals, Metals Park, Ohio, USA).

15 **Hollingsworth, E. H.** and **Hunsicker, H.** *Metals handbook*, vol. 13, 1987, p. 583 (ASM International, Metals Park, Ohio, USA).

16 **Buchheit, R. G.** A compilation of corrosion potentials reported for intermetallic phases in aluminum-alloys. *J. Electrochem. Soc.*, 1995, **142**, 3994–3996.

17 **Mazurkiewicz, B.** and **Piotrowski, A.** The electrochemical behaviour of the Al_2Cu intermetallic compound. *Corros. Sci.*, 1983, **23**, 697.

18 **Mazurkiewicz, B.** Electrochemical behavior of the Al_8Mg_5 intermetallic compound. *Corros. Sci.*, 1983, **23**, 687.

19 **Scully, J. R., Knight, T. O., Buchheit, R. G.,** and **Peebles, D. E.** Electrochemical characteristics of the Al_2Cu, Al_3Ta and Al_3Zr intermetallic phases and their relevancy to the localized corrosion of Al alloys. *Corros. Sci.*, 1993, **35**, 185.

20 **Buchheit, R. G., Grant, R. P., Hlava, P. F., McKenzie, B.,** and **Zender, G. L.** Local dissolution phenomena associated with S phase (Al_2CuMg) particles in aluminum alloy 2024-T3. *J. Electrochem. Soc.*, 1997, **144**, 2621.

21 **Buchheit, R. G., Moran, J. P.,** and **Stoner, G. E.** Localized corrosion behavior of alloy 2090 – the role of microstructural heterogeneity. *Corrosion*, 1990, **46**, 610.

22 **Wang, M. F., Li, X. G., Dub, N., Huang, Y. Z.,** and **Korsunsky, A.** Direct evidence of initial pitting corrosion. *Electrochem. Commun.*, 2008, **10**, 1000–1004.

23 **Chlistovsky, R. M., Heffernan, P. J.,** and **DuQuesnay, D. L.** Corrosion-fatigue behaviour of 7075-T651 aluminum alloy subjected to periodic overloads. *Int. J. Fatigue*, 2007, **29**, 1941–1949.

24 **Ciccone, M. P., Gangloff, R. P.,** and **Kelly, R. G.** Test environment selection for corrosion-fatigue testing of aluminum alloy 7075-T6. *Corrosion*, 2005, **61**, 571–578.

25 **Liu, Y., Arenas, M. A., Skeldon, P., Thompson, G. E., Bailey, P., Noakes, T. C. Q., Habazaki, H.,** and **Shimizu, K.** Anodic behaviour of a model second phase: Al-20at.%Mg-20at.%Cu. *Corros. Sci.*, 2006, **48**, 1225–1248.

26 **de Miera, M. S., Curioni, M., Skeldon, P.,** and **Thompson, P. G. E.** Investigation of the corrosion behaviour of AA 2024-T3 in low concentrated chloride media. *Corros. Sci.*, 2008, **50**, 2646–2657.

27 **Pidaparti, R. M.** Structural corrosion health assessment using computational intelligence methods. *Struct. Health Monit.*, 2007, **6**, 245–259.

28 **Shelekhov, E. V.** and **Sviridova, T. A.** Programs for x-ray analysis of polycrystals. *Metal Sci. Heat Treat.*, 2000, **42**, 309–313.

29 **Cabot, P. L., Perez, E.,** and **Virgili, J.** Oxide dissolution during galvanostatic oxidation of aluminum. *Anal. de Quim. Ser. A-Quim. Fis. Y Quim. Tec.*, 1985, **81**, 434–436.

30 **Smith, R. A.** Fine-tuning the eddy current detection of hidden first-layer corrosion in aircraft skins. *Insight*, 1998, **40**, 712–721.

31 **Freyman, L. I.** Kinetics of metal pitting corrosion. In *Corrosion and protection*, 1985, pp. 3–71 (VINITI, Moscow).

32 **Sinyavsky, V. S., Val'kov, V. D.,** and **Budov, G. M.** *Corrosion and protection of aluminium alloys*, 1979 (Metallurgiya, Moscow).

33 **Kelly, A.** and **Nicholson, R. B.** *Strengthening methods in crystals*, 1971 (Elsevier, London).

34 **Pourbaix, M.** *Lectures on electrochemical corrosion*, 1973 (Plenum Press, New York).

35 **Garz, J.** and **Schatt, W.** Zeitschrift für physikalische. *Chemie*, 1969, **B240**, 371–379.

36 **Vasiliev, V. Y., Kukolkin, A. G., Bayankin, V. Y., Gromov, M. S.,** and **Volkov, V. A.** The variation of corrosion susceptibility of aluminium alloys during exploitation. *Met. Prot.*, 1995, **31**, 16–20.